

Attosecond Time-Domain Measurement of Core-Level-Exciton Decay in Magnesium Oxide

Romain Géneaux^{1,*}, Christopher J. Kaplan^{1,*}, Lun Yue², Andrew D. Ross¹, Jens E. Bækhoj², Peter M. Kraus¹, Hung-Tzu Chang¹, Alexander Guggenmos¹, Mi-Ying Huang¹, Michael Zürch¹, Kenneth J. Schafer², Daniel M. Neumark^{1,3}, Mette B. Gaarde² and Stephen R. Leone^{1,4,3,‡}

¹*Department of Chemistry, University of California, Berkeley, California 94720, USA*

²*Department of Physics and Astronomy, Louisiana State University, Baton Rouge, Louisiana 70803, USA*

³*Chemical Sciences Division, Lawrence Berkeley National Laboratory, Berkeley, California 94720, USA*

⁴*Department of Physics, University of California, Berkeley, California 94720, USA*

 (Received 27 December 2019; revised manuscript received 25 March 2020; accepted 28 April 2020; published 21 May 2020)

Excitation of ionic solids with extreme ultraviolet pulses creates localized core-level excitons, which in some cases couple strongly to the lattice. Here, core-level-exciton states of magnesium oxide are studied in the time domain at the Mg $L_{2,3}$ edge with attosecond transient reflectivity spectroscopy. Attosecond pulses trigger the excitation of these short-lived quasiparticles, whose decay is perturbed by time-delayed near-infrared pulses. Combined with a few-state theoretical model, this reveals that the infrared pulse shifts the energy of bright (dipole-allowed) core-level-exciton states as well as induces features arising from dark core-level excitons. We report coherence lifetimes for the two lowest core-level excitons of 2.3 ± 0.2 and 1.6 ± 0.5 fs and show that these are primarily a consequence of strong exciton-phonon coupling, disclosing the drastic influence of structural effects in this ultrafast relaxation process.

DOI: [10.1103/PhysRevLett.124.207401](https://doi.org/10.1103/PhysRevLett.124.207401)

Excitation of a solid with a high-energy photon leads to an ultrafast dynamic response involving structural and electronic degrees of freedom. In the frequency domain, these processes can be studied by comparing the absorption and emission spectra of the system, which, respectively, reveal which states were excited and eventually populated, as is done, for instance, in resonant inelastic x-ray scattering [1]. This grants indirect access to the behavior of the transient core-level-excited state. In contrast, the development of attosecond science now offers an unmediated view of this dynamics in the time domain [2,3], where intermediate states involved in the decay can be directly probed. For instance, in attosecond transient absorption spectroscopy [4,5], short extreme ultraviolet (XUV) pulses can be used to precisely trigger the core-hole excitation, whose decay is then tracked with optical femtosecond laser pulses [6,7].

In the condensed phase, an important question arises: Can nuclear motion influence the decay of the core-hole for states living only a few femtoseconds? Intuitively, one might expect that if the Auger or radiative lifetime of an intermediate state Γ^{-1} is short compared to a relevant phonon period τ_{ph} , the lattice will not have time to respond to the creation of the core hole, and the lattice will not contribute. Early photoemission studies of ionic insulators disproved this argument, measuring substantial spectral broadening linked to coupling between the core hole and optical phonons [8–10]. The time-domain evolution of the

core-level-excited state in these conditions, however, has yet to be explored.

In this Letter, XUV attosecond transient reflectivity spectroscopy (ATRS) is used to investigate the core-level-excited dynamics of magnesium oxide (MgO). In this ionic insulator, the low dielectric constant and the positive charge of Mg atoms mean that a Mg core hole is very weakly screened. This contributes to the formation of core-level excitons—bound electron-hole pairs—at the Mg $L_{2,3}$ edge [11,12]. First, several core-level excitons are identified, and their linewidths are shown to be dominated by phonon broadening, indicating a substantial exciton-phonon coupling. Then, the core-level excitons are initiated by an XUV pulse, and a short near-infrared (NIR) laser pulse probes their decay. The NIR and core-level-exciton interaction is interpreted using a few-level theoretical model, whose agreement with the experiment allows us to identify two effects of the NIR pulse: (i) resonant and nonresonant coupling of the various excitonic states and (ii) creation of light-induced features interpreted as the manifestation of dark excitonic states. The decays of the two lowest-energy core-level excitons are extracted, showing coherence lifetimes below 3 fs. Finally, the link between these features and exciton-phonon coupling is discussed.

The experiment was performed on a single-crystalline commercial sample of MgO(100) (MTI Corporation) featuring industrial-grade polishing (rms < 10 Å) and a crystalline purity > 99.95%. Given that the samples are thick (0.5 mm),

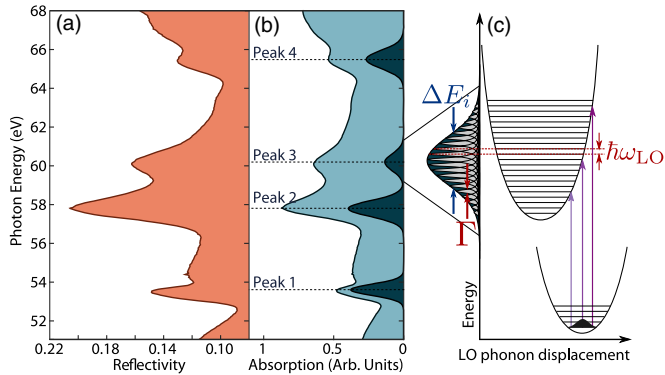


FIG. 1. Absolute reflectivity at the Mg $L_{2,3}$ edge in MgO(100). (a) Measurement at 66° from normal incidence. (b) Absorption coefficient obtained by Kramers-Kronig analysis (light blue), with four peaks visible (dotted lines) fitted to Gaussian distributions (dark blue). (c) Schematic of linear exciton-phonon coupling along the LO phonon coordinate. In the strong coupling regime, the absorption line shape of the i th exciton is a Gaussian of width ΔE_i . It is composed of a series of Lorentzians of width Γ , spaced by $\hbar\omega_0$, the phonon energy.

the investigation mandates the use of ATRS [13], which does not require thin films, contrary to transmission experiments. Broadband pulsed XUV attosecond radiation covering a continuous span of 20–70 eV is produced by high harmonic generation in argon using 480 μJ , sub-5-fs NIR pulses centered at 750 nm at a repetition rate of 1 kHz. After filtering the NIR light with a 100-nm-thick aluminum film, the XUV pulse is reflected by the sample at an incidence angle of 66° from normal. The reflected light is then dispersed and imaged onto a CCD camera (Princeton Instruments). The spectral resolution at 50 eV is $\sigma = 25$ meV as determined using atomic absorption lines. In the time-resolved experiment, a strong 4.5 fs pulse of NIR light perturbs the system following the core-hole creation by the XUV pulse. At each time delay between the XUV and NIR pulses, the reflectivity R_{on} (respectively, R_{off}) is measured with 100 ms integration time with the NIR beam on (respectively, off). The transient reflectivity $dR/R = (R_{\text{on}} - R_{\text{off}})/R_{\text{off}}$ is computed and averaged over 100 full time-delay scans. The slow drift of the pump-probe delay is stabilized over several hours using periodic reference measurements [14]. In all data presented here, the XUV and NIR pulses are s and p polarized with respect to the sample surface, respectively [15].

Figure 1(a) shows the XUV reflectivity of the MgO crystal in the absence of the NIR pulse. During the measurement, the reflectivity of MgO and a calibrated gold mirror are taken sequentially, allowing signal normalization and thus obtaining the absolute reflectivity of MgO. To allow a more direct interpretation, the absorption spectrum, shown in Fig. 1(b), is obtained by a Kramers-Kronig (KK) analysis: The data are padded with literature data [16] covering the infrared to x-ray regions, which allows

performing the KK integral over a wide frequency range. Four peaks are measured on top of a continuum originating in transitions to the conduction band, whose minimum lies at 53.72 eV [12]. As explained in Supplemental Material [17], peaks 1 and 2 correspond to core-level excitons, while the excitonic nature of peaks 3 and 4 is less direct. Density-functional calculations suggest that peak 1 has prevailing s character, while the others are of mixed s - d character [24]. After removal of the continuous background by a procedure detailed in Supplemental Material [17], the peaks can be fitted to Gaussian line shapes with peak energies matching the literature within 0.5% or less [25] and full width at half maximum (FWHM) of $\Delta E_{1-4} = 0.68, 0.95, 1.03,$ and 1.10 eV, from low to high energy, respectively. The Mg $2p$ hole involved here is known to be filled almost solely by intra-atomic Auger processes [26], which by itself would give a narrow Lorentzian line shape with at most $\Gamma_{2p} = 30$ meV [27,28], at clear variance with the experiment. In addition, since the sample is monocrystalline, we can safely disregard inhomogeneous broadening that would be caused by site-to-site fluctuations of the exciton energy in a disordered sample. Therefore, the broad Gaussian linewidths must be caused by strong exciton-phonon coupling, as represented in Fig. 1(c) and as already recognized for the lowest-energy exciton [12]. Mahan [30] showed that in crystals with halite structure, such as MgO, core-level excitons couple mainly to the longitudinal optical (LO) phonon at the X point. For MgO, this phonon has an energy of $\omega_{\text{LO}} = 60$ meV [31]. After deconvolution of the Auger linewidth and the spectral resolution of the experiment, the phonon broadening of each exciton is equivalent to 11.1, 15.7, 16.7, and 17.9 phonons, from low to high energy, respectively. This strong coupling is the result of the ionicity of MgO: The principal way of screening the hole on the Mg cation is the motion of neighboring anions.

The transient reflectivity of the system is shown in Fig. 2(a), where negative times mean the XUV comes first. Strong modifications of the reflectivity are seen mostly around the region of temporal overlap, which lasts 4–5 fs in time delay. Remarkably, no changes are observed after temporal overlap (for delays larger than 10 fs), which is where signals created by the NIR and probed by the XUV would appear. The absence of such features, commonly observed in semiconductors [13,32,33], allows us to disregard carrier excitation by the NIR pulse across the 7.8 eV band gap of MgO. On the other hand, changes before $\tau = 0$ are observed for peaks 1 and 2. They correspond to XUV-triggered dynamics probed by the NIR pulse and are a direct time-domain observation of the core-level-excited state decay, consistent with the excitonic nature of peaks 1 and 2. The transient reflectivity signal extends only a few femtoseconds before $\tau = 0$, indicating that the excitonic states experience a very fast dephasing mechanism. This observation demonstrates the ability of attosecond spectroscopy to capture the dynamics of extremely short-lived

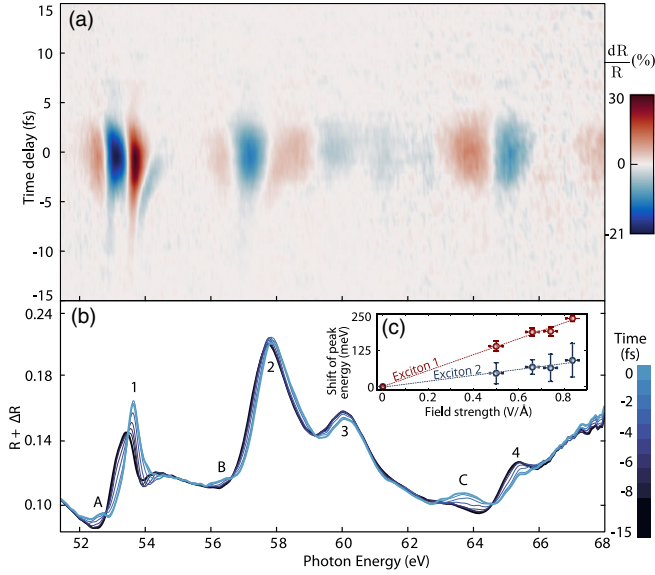


FIG. 2. Attosecond-resolved dynamics of excitons in MgO. (a) Time-delay-dependent transient reflectivity, measured with a probe field strength of $0.84 \pm 0.01 \text{ V}/\text{\AA}$, or $(9.3 \pm 0.2) \times 10^{12} \text{ W}/\text{cm}^2$. (b) Absolute reflectivity, obtained by adding the static and differential ones, for pump-probe delays from -15 to 0 fs. Features corresponding to excitonic shifts (1–4), and light-induced features (A–C) are indicated. (c) Energy shift of excitons 1 (red line) and 2 (blue line) at $\tau = 0$ as a function of the NIR field strength. The dotted lines are linear fits, giving shifts of 274 and $101 \text{ meV}/(\text{V}/\text{\AA})$, respectively.

core-level-excited states in the condensed phase, as was previously done for longer-lived states in atomic species [34–38].

Figure 2(b) shows the absolute reflectivity of MgO at different pump-probe delays. We identify three types of features with distinct behaviors: (i) peaks 1 and 2 experience a blueshift near zero delay; (ii) the reflectivities of peaks 3 and 4 decrease; (iii) new features, marked as A–C, emerge at energies where no signal was initially present. While the first two trends were already recognized by Moulet *et al.* [39] in SiO_2 , features A–C show a strikingly different behavior: They do not seem to originate from either of the core-level excitons but rather appear only in the presence of the strong NIR field.

The experiment was repeated while varying the strength of the NIR electric field, resulting in a linear increase of the blueshifts of excitons 1 and 2 [Fig. 2(c)], with significantly different polarizabilities between excitons 1 and 2. This behavior is distinct from the optical Stark effect of one core-level exciton coupled only to a continuum, whose shift would increase linearly with NIR intensity at large pump detunings [40]. NIR-driven couplings between excitonic levels must therefore play an important role here. Finally, our experiment did not reveal any change in the dynamics when the polarization angle of either the pump or probe beam was varied.

We attempt to disentangle the two types of exciton dynamics driven by the phonon- and the NIR-driven couplings, respectively, via a simple model for the core-level-exciton system interacting with a two-color XUV and NIR pulse. Given that the excitonic states originate in spatially localized bound electron-hole pairs, they are similar in character to atomic states. We thus start by constructing a four-level system consisting of the ground state 0 , excitons 1 and 2 (which exhibit the most intense behavior), and a so-called dark exciton state d that has no dipole coupling to the ground state but can couple by the NIR pulse to both exciton states. Although we do not predetermine the energy of the dark state (we will later extract this energy by fitting the model calculations to the experimental results), we do assume the dark state is in the vicinity of the other exciton states. Solving the time-dependent Schrödinger equation (TDSE) for this system yields a time-dependent dipole moment of the form

$$D(t, \tau) \propto 2\text{Re}(c_0^* c_1 \mu_{0,1} e^{i\phi_1(t,\tau)} + c_0^* c_2 \mu_{0,2} e^{i\phi_2(t,\tau)} + c_1^* c_d \mu_{1,d} e^{i\phi_1(t,\tau)} + c_2^* c_d \mu_{2,d} e^{i\phi_2(t,\tau)}), \quad (1)$$

where the subscripts 0 , 1 , 2 , and d denote the four states, τ is the XUV-NIR delay, $\mu_{i,j}$ are the transition dipole moments, and c_i are the delay- and time-dependent amplitudes of the four states.

The exciton phases ϕ_1 and ϕ_2 are added to the dipole in order to account for three dynamical effects that go beyond the four-level TDSE model, at the phenomenological level: $\phi_i(t, \tau) = i\Gamma_{2p}t + \phi_L(t, \tau) + \phi_{\text{ph},i}(t)$, where $\Gamma_{2p} = 30 \text{ meV}$ [27] is the $2p$ core-hole Auger decay rate, $\phi_L(t)$ is the ac Stark phase imposed by laser dressing of the loosely bound exciton states, and $\phi_{\text{ph},i}(t)$ is due to the phonon coupling. The ac Stark phase is proportional to the energy shift U_p experienced by a free electron in an oscillating field:

$$\phi_L(t, \tau) = -\beta \int_0^t U_p(t', \tau) dt', \quad (2)$$

and β is determined via fitting as described below. The exciton-phonon coupling phase is given by [10]

$$\phi_{\text{ph},i}(t) = i \frac{M_i^2}{\omega_{\text{LO}}^2} [(2N + 1)(1 - \cos \omega_{\text{LO}}t) - i(\omega_{\text{LO}}t - \sin \omega_{\text{LO}}t)], \quad (3)$$

where N is the thermal phonon population, $\omega_{\text{LO}} = 60 \text{ meV}$ is the LO phonon energy [31], and M_i is the exciton-phonon coupling constant, to be determined by the fit. Finally, the absorption spectrogram is calculated as $A(\omega, \tau) = -\omega \text{Im}[E_{\text{XUV}}^*(\omega) \tilde{d}(\omega, \tau)]$, with $E_{\text{XUV}}(\omega)$ and $\tilde{D}(\omega, \tau)$ the Fourier transforms of the XUV electric field and $D(t, \tau)$, respectively [41]. This is compared to the experimental transient absorption trace shown in Figs. 3(a) and 3(b), which

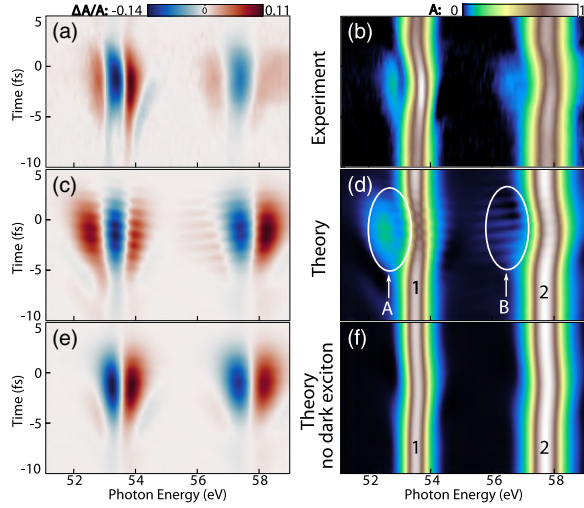


FIG. 3. Transient experimental (a),(b) and calculated (c),(f) absorption spectra. The experimental spectrograms are obtained from KK analysis of Fig. 2(a). (a),(c),(e) and (b),(d),(f) show changes in absorption and absolute absorption, respectively. Results from calculations are normalized to the same scale as experiments. (e),(f) show a calculation in which the dark state is omitted.

was obtained by KK analysis of transient reflectivity data (see Supplemental Material [17]).

The parameters used in the model are extracted in two stages. We first fit the calculated XUV-alone spectrum to the experimental spectrum to obtain the phonon coupling constants $M_1 = 266.3 \pm 8.0$ meV and $M_2 = 366.7 \pm 7.1$ meV, and $\mu_{0,2} = -0.0818 \pm 0.0013$ a.u. (when using $\mu_{0,1} = 0.05$ a.u. as an overall scaling parameter). The parameters characterizing the laser-driven couplings are found by fitting the measured spectrum in the interval [51.1, 59.1 eV], at overlap ($\tau = 0$), to that calculated by using the measured NIR pulse shape as input, with a peak intensity of 2×10^{12} W/cm², and averaging over approximately one NIR optical cycle around $\tau = 0$. A full delay-dependent calculation is then performed using the extracted parameters. The main discrepancy in the result is the appearance of subcycle oscillations in the theoretical absorption, which are not resolved in the experimental delay scan. We speculate that this is due to experimental factors such as time-delay jitter or phase slip effects between NIR and XUV, possibly important in reflectivity geometry. For this reason, a half-cycle moving average is added to the calculation. Even though the oscillations do not completely disappear, this allows a clearer comparison, as shown in Figs. 3(c) and 3(d).

The comparison between experiment and theory is otherwise good, with the dynamics of both the excitonic blueshifts and the A-B features reproduced well. There are several important lessons learned from the comparison: First, the presence of the dark state is crucial for the appearance of features A and B. This is demonstrated in

Figs. 3(e) and 3(f), which show the calculated spectrogram in the absence of the dark state. The energy of the dark state is found to be 54.4 ± 0.3 eV, i.e., located between excitons 1 and 2, so that features A and B are one NIR photon energy below and above the dark state, respectively. This suggests that A and B are light-induced states (LISs) that can be understood as the intermediate state in two-photon XUV + NIR transitions from the ground to the dark state. LISs are well known from atomic transient absorption studies [42–44] but have not previously been observed in the solid state. We find that the dark-state coupling matrix elements are large (similar to those between atomic states [45]) and comparable in magnitude to each other, $\mu_{1,d} = 3.8 \pm 0.5$ a.u. and $\mu_{d,2} = -3.7 \pm 1.0$ a.u. [46], and that $\beta = 1 \pm 0.5$.

The fact that the NIR-induced attosecond excitonic dynamics are well described using concepts from atomic physics highlights the striking similarity between excitons and isolated atoms. However, the way these quasiparticles decay is remarkably different for the solid versus atoms. Indeed, the Mahan model that we use to describe exciton-phonon coupling [phonon phase in Eq. (3)] predicts a Gaussian decay of the dipole moment for short times: $e^{-\text{Im}(\phi_{\text{ph}})} \propto e^{-M_i^2 t^2}$ for $\omega_{\text{LO}} t \ll 1$. Thus, in the framework of this model, the excitonic coherence lifetime is directly reduced by the strength of the exciton-phonon coupling. To validate the use of this model in our case, we compare its result to the experimental data. The center energy of excitons 1 and 2 is measured as a function of pump delay, and the result is fitted as the convolution of the NIR intensity and an unknown dipole decay for each exciton. Figure 4 shows that the comparison of this fit to the theoretical model is reasonable, yielding coherence decay times at half maximum of 2.3 ± 0.2 and 1.6 ± 0.5 fs. Including either just the Auger or just the phonon dephasing decay (Fig. 4) shows that the exciton decay is dominated by the exciton-phonon coupling.

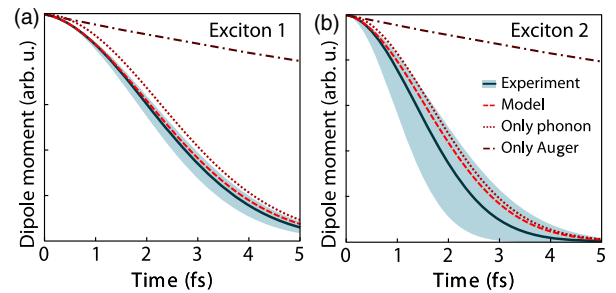


FIG. 4. Dipole decays obtained from the delay-dependent energy position of excitons 1 (a) and 2 (b) (full blue lines). The shaded areas represent the 95% confidence interval of the fitting in addition to a ± 0.5 fs uncertainty on the NIR pulse duration. The experimentally obtained dipole decay is compared with the full model (dashed red line), and the model with only the phonon contribution (dotted line) or with only the Auger decay (dash-dotted line).

Returning now to the static absorption profiles of Fig. 1, the Gaussian linewidths ΔE_1 and ΔE_2 correspond to dephasing times of 2.6 ± 0.3 and 1.9 ± 0.4 fs, respectively. The similarity between these values and the dephasing times measured in the time domain indicates that exciton lifetimes in MgO are mainly governed by exciton-phonon coupling. We interpret this finding as an analog of *vibrational-lifetime interferences* observed in small molecules [47,48]: Since Γ_{2p} is on the same order of magnitude as ω_{LO} , phonons can influence the excitonic decays on time-scales much shorter than the phonon period (69 fs, in our case). Here, the substantial exciton-phonon coupling manifests as a spectacularly fast dephasing of the core-level-excited state. We expect the findings presented here to have important ramifications in the time-domain study of similar short-lived core-level-excited states in the condensed phase.

In summary, we investigated the decay of core-level-excited states in MgO(100) using ATRS. Using a short NIR field to perturb the relaxation, excitonic blueshifts and light-induced states were identified as distinctive features of the exciton-NIR interaction. The coherence lifetimes of the excitons were found to be principally given by the inverse width of the vibronic wave packet created in the core-level-excited state. This study furthers the understanding of light-induced modification of short-lived excitonic states and extends concepts of attosecond metrology to the solid state. It presents a direct measurement of an extremely short natural lifetime obtained using attosecond transient spectroscopy. Furthermore, the observation of substantial phonon dephasing is of compelling importance for future attosecond studies, which are making progress in the understanding of condensed phase systems such as solids and solvated molecules.

The authors thank Eric M. Gullikson for performing the calibration of the gold mirror and are grateful to L. Barreau and H. Marroux for comments on the manuscript. Experimental investigations were supported by the Defense Advanced Research Projects Agency PULSE Program Grant No. W31P4Q-13-1-0017, the U.S. Air Force Office of Scientific Research No. FA9550-14-1-0154, the Army Research Office Multidisciplinary University Research Initiative (MURI) Grant No. WN911NF-14-1-0383, and the W.M. Keck Foundation No. 046300. Theoretical work at L. S. U. was supported by U.S. Department of Energy, Office of Science, Basic Energy Sciences, under Contract No. DE-SC0010431.

*These authors contributed equally to this work.

†rgeneaux@berkeley.edu

‡srl@berkeley.edu

- [1] L. J. P. Ament, M. van Veenendaal, T. P. Devereaux, J. P. Hill, and J. van den Brink, *Rev. Mod. Phys.* **83**, 705 (2011).
 [2] F. Krausz and M. Ivanov, *Rev. Mod. Phys.* **81**, 163 (2009).

- [3] K. Ramasesha, S. R. Leone, and D. M. Neumark, *Annu. Rev. Phys. Chem.* **67**, 41 (2016).
 [4] P. M. Kraus, M. Zürich, S. K. Cushing, D. M. Neumark, and S. R. Leone, *Nat. Rev. Chem.* **2**, 82 (2018).
 [5] R. Généaux, H. J. B. Marroux, A. Guggenmos, D. M. Neumark, and S. R. Leone, *Phil. Trans. R. Soc. A* **377**, 20170463 (2019).
 [6] A. Chew, N. Douguet, C. Cariker, J. Li, E. Lindroth, X. Ren, Y. Yin, L. Argenti, W. T. Hill, and Z. Chang, *Phys. Rev. A* **97**, 031407(R) (2018).
 [7] A. R. Beck, B. Bernhardt, E. R. Warrick, M. Wu, S. Chen, M. B. Gaarde, K. J. Schafer, D. M. Neumark, and S. R. Leone, *New J. Phys.* **16**, 113016 (2014).
 [8] P. H. Citrin, P. Eisenberger, and D. R. Hamann, *Phys. Rev. Lett.* **33**, 965 (1974).
 [9] C. O. Almbladh, *Phys. Rev. B* **16**, 4343 (1977).
 [10] G. D. Mahan, *Phys. Rev. B* **15**, 4587 (1977).
 [11] T. Lindner, H. Sauer, W. Engel, and K. Kambe, *Phys. Rev. B* **33**, 22 (1986).
 [12] W. L. O'Brien, J. Jia, Q. Y. Dong, T. A. Callcott, J. E. Rubensson, D. L. Mueller, and D. L. Ederer, *Phys. Rev. B* **44**, 1013 (1991).
 [13] C. J. Kaplan, P. M. Kraus, A. D. Ross, M. Zürich, S. K. Cushing, M. F. Jager, H.-T. Chang, E. M. Gullikson, D. M. Neumark, and S. R. Leone, *Phys. Rev. B* **97**, 205202 (2018).
 [14] M. F. Jager, C. Ott, C. J. Kaplan, P. M. Kraus, D. M. Neumark, and S. R. Leone, *Rev. Sci. Instrum.* **89**, 013109 (2018).
 [15] In all data presented here, *s*-polarized XUV and *p*-polarized NIR (with respect to the sample) are used, as they, respectively, provide more XUV reflectivity and reduced noise from stray reflected NIR.
 [16] D. Roesler and D. Huffman, in *Handbook of Optical Constants of Solids* (Elsevier, New York, 1997), pp. 919–955.
 [17] See Supplemental Material at <http://link.aps.org/supplemental/10.1103/PhysRevLett.124.207401> for additional details on the excitonic nature of peaks, the background subtraction procedure, and the Kramers-Kronig analysis of static and transient data, which includes Refs. [18–23].
 [18] S.-D. Mo and W. Y. Ching, *Phys. Rev. B* **62**, 7901 (2000).
 [19] T. Mizoguchi, K. Tatsumi, and I. Tanaka, *Ultramicroscopy* **106**, 1120 (2006).
 [20] T. S. Robinson, *Proc. Phys. Soc. London Sect. B* **65**, 910 (1952).
 [21] D. M. Roessler, Br., *J. Appl. Phys.* **16**, 1359 (1965).
 [22] F. Quéré, S. Guizard, P. Martin, G. Petite, O. Gobert, P. Meynadier, and M. Perdrix, *Appl. Phys. B* **68**, 459 (1999).
 [23] R. L. Sutherland, *Handbook of Nonlinear Optics* (Marcel Dekker, New York, 1996).
 [24] C. Elsässer and S. Köstlmeier, *Ultramicroscopy* **86**, 325 (2001).
 [25] V. E. Henrich, G. Dresselhaus, and H. J. Zeiger, *Phys. Rev. Lett.* **36**, 158 (1976).
 [26] P. H. Citrin, *J. Electron Spectrosc. Relat. Phenom.* **5**, 273 (1974).
 [27] P. H. Citrin, G. K. Wertheim, and Y. Baer, *Phys. Rev. B* **16**, 4256 (1977).
 [28] While the natural linewidth of Mg *2p* is unknown for MgO, we can use the value for Mg metal as an upper limit [29]. Indeed, the core-hole decays predominantly by a LVV

- Auger process, meaning that this linewidth will be even smaller in MgO in which the electronic density is reduced around Mg atoms.
- [29] W.L. O'Brien, J. Jia, Q.-Y. Dong, T. A. Callcott, K. E. Miyano, D. L. Ederer, D. R. Mueller, and C.-C. Kao, *Phys. Rev. B* **47**, 140 (1993).
- [30] G. D. Mahan, *Phys. Rev. B* **21**, 4791 (1980).
- [31] R. K. Singh and K. S. Upadhyaya, *Phys. Rev. B* **6**, 1589 (1972).
- [32] M. Zürch, H.-T. Chang, L. J. Borja, P. M. Kraus, S. K. Cushing, A. Gandman, C. J. Kaplan, M. H. Oh, J. S. Prell, D. Prendergast, C. D. Pemmaraju, D. M. Neumark, and S. R. Leone, *Nat. Commun.* **8**, 15734 (2017).
- [33] F. Schlaepfer, M. Lucchini, S. A. Sato, M. Volkov, L. Kasmí, N. Hartmann, A. Rubio, L. Gallmann, and U. Keller, *Nat. Phys.* **14**, 560 (2018).
- [34] A. R. Beck, B. Bernhardt, E. R. Warrick, M. Wu, S. Chen, M. B. Gaarde, K. J. Schafer, D. M. Neumark, and S. R. Leone, *New J. Phys.* **16**, 113016 (2014).
- [35] W. Cao, E. R. Warrick, A. Fidler, D. M. Neumark, and S. R. Leone, *Phys. Rev. A* **94**, 053846 (2016).
- [36] S. Beaulieu, E. Bloch, L. Barreau, A. Comby, D. Descamps, R. Généaux, F. Légaré, S. Petit, and Y. Mairesse, *Phys. Rev. A* **95**, 041401(R) (2017).
- [37] C. Ott, A. Kaldun, P. Raith, K. Meyer, M. Laux, J. Evers, C. H. Keitel, C. H. Greene, and T. Pfeifer, *Science* **340**, 716 (2013).
- [38] C. Ott, A. Kaldun, L. Argenti, P. Raith, K. Meyer, M. Laux, Y. Zhang, A. Blättermann, S. Hagstotz, T. Ding, R. Heck, J. Madroñero, F. Martín, and T. Pfeifer, *Nature (London)* **516**, 374 (2014).
- [39] A. Moulet, J. B. Bertrand, T. Klostermann, A. Guggenmos, N. Karpowicz, and E. Goulielmakis, *Science* **357**, 1134 (2017).
- [40] M. Combescot, *Phys. Rep.* **221**, 167 (1992).
- [41] M. B. Gaarde, C. Buth, J. L. Tate, and K. J. Schafer, *Phys. Rev. A* **83**, 013419 (2011).
- [42] S. Chen, M. J. Bell, A. R. Beck, H. Mashiko, M. Wu, A. N. Pfeiffer, M. B. Gaarde, D. M. Neumark, S. R. Leone, and K. J. Schafer, *Phys. Rev. A* **86**, 063408 (2012).
- [43] M. Justine Bell, A. R. Beck, H. Mashiko, D. M. Neumark, and S. R. Leone, *J. Mod. Opt.* **60**, 1506 (2013).
- [44] M. Chini, X. Wang, Y. Cheng, Y. Wu, D. Zhao, D. A. Telnov, S. I. Chu, and Z. Chang, *Sci. Rep.* **3**, 1105 (2013).
- [45] M. Wu, S. Chen, S. Camp, K. J. Schafer, and M. B. Gaarde, *J. Phys. B* **49**, 062003 (2016).
- [46] In the fit, we cannot distinguish between whether the signs of $\mu_{1,d}$ and $\mu_{d,2}$ are the same or opposite. Choosing initial conditions of same signs yields a dark state energy and matrix elements of the same order of magnitude.
- [47] F. Kaspar, W. Domcke, and L. S. Cederbaum, *Chem. Phys.* **44**, 33 (1979).
- [48] F. K. Gel'Mukhanov, L. N. Mazalov, and A. V. Kondratenko, *Chem. Phys. Lett.* **46**, 133 (1977).